Available online at www.sciencedirect.com
ScienceDirect
Journal of Sound and Vibration 307 (2007) 265–279
JOURNAL OF SOUND AND VIBRATION
www.elsevier.com/locate/jsvi

Eigenvalue analysis and optimised numerical simulations of the space shuttle remote manipulator system

Simon M. Wiedemann[a,*], Colin L. Kirk[b]

[a]*University of Applied Sciences, Munich, Germany*
[b]*College of Aeronautics, Cranfield University, UK*

Received 21 October 2006; received in revised form 28 June 2007; accepted 2 July 2007

Abstract

This paper extends the earlier work of various researchers and the authors and gives an analytical solution to the natural frequencies and mode shapes of the space shuttle remote manipulator system (SRMS). For optimised numerical simulations, the exact eigenmodes are replaced by simple polynomials for use in Lagrange's equation. The close agreement of the lowest natural frequency by both methods for various fixed SRMS configurations, being almost independent over the range, shows that simple mode shapes can be used to determine transient vibrations induced by large angle slews of the SRMS and payload system. The use of a tangent frame formulation for each link relative to its revolute joint is the key for the formulation of the flexible link boundary conditions and is more realistic than the use of arbitrary beam functions by other authors.

1. Introduction

Throughout the last two or more decades a considerable quantity of research has been devoted to the dynamics and vibration control of multi-link robotic manipulators, subjected to disturbances arising for example from rotational manoeuvres by torque motors about revolute joints. Of particular interest is the vibration of flexible space robotic systems, such as the space shuttle remote manipulator system (SRMS) and the space station mobile remote manipulator system (MRMS). These structures are lightweight and very flexible, in contrast to stiff industrial robots.

A sample of the relevant literature on the SRMS is given in Refs. [1–12], but most papers give only little detailed information about the operation of the SRMS or its dynamic characteristics, with the exception of Refs. [5,9,13], which give a few numerical results. Two of the major concerns are possible fatigue damage in the high reduction gear trains [1] and residual vibrations following a SRMS manoeuvre [5,9].

*Corresponding author.
E-mail address: Simon.Wiedemann@fhm.edu (S.M. Wiedemann).

0022-460X/$ - see front matter © 2007 Elsevier Ltd. All rights reserved.
doi:10.1016/j.jsv.2007.07.002

Previous research work [14,15] has analysed single-flexible link robots, taking account of end payload inertia and mass, shoulder drive or hub inertia and various restraints by springs, but these papers only consider small point masses as payloads and torsional flexibility only between the hub and the motor rotor [16] presents an analytical solution for the natural frequencies and mode shapes of a free–free planar beam subject to arbitrary kinematic and kinetic boundary conditions.

A three-link system has been studied by Kwak and Meirovitch [17] using assumed mode shapes and allowing for planar rigid body Shuttle motion, but no justification is for the use of the approximate mode shapes. Wiedemann [18] considers the natural frequencies and mode shapes of an arbitrary structure of Euler–Bernoulli beams subject to arbitrary kinematic and kinetic boundary conditions and is an extension of research work carried out in Refs. [19,20]. The latter developed the method that was later generalised in Ref. [18] for the SRMS, but did not give the mode shape orthogonality conditions or consider numerical accuracy and optimisation of numerical simulations.

2. Exact analytical solution for SRMS natural frequencies

The SRMS consists basically of two flexible links and a very stiff end effector connected by revolute joints. All three joints can be unlocked so as to be driven by high reduction ratio gear trains or locked, having joint flexibility.

Fig. 1 shows that the SRMS is idealised as two flexible beams L_1 and L_2 with a rigid end effector L_3 connected to a rigid payload of mass M_p and moment of inertia I_p. The standard solution to the beam differential equation yields the mode shape of each beam as

$$W_i(x) = A_i \sin(k_i x) + B_i \cos(k_i x) + C_i \sinh(k_i x) + D_i \cosh(k_i x), \tag{1}$$

where

$$k_i^2 = \omega_n \sqrt{\frac{m_{bi}}{EI_i}}, \quad i = 1, 2. \tag{2}$$

and m_{bi} is the mass per unit length of link i and EI_i its flexural stiffness.

Eq. (1) is solved for the two coupled links using the bending moment and shear force boundary conditions at $x_i = 0$ and L_i corresponding to O_1, O_2 and O_3 in Fig. 1. The 2×4 boundary conditions yield 8 equations,

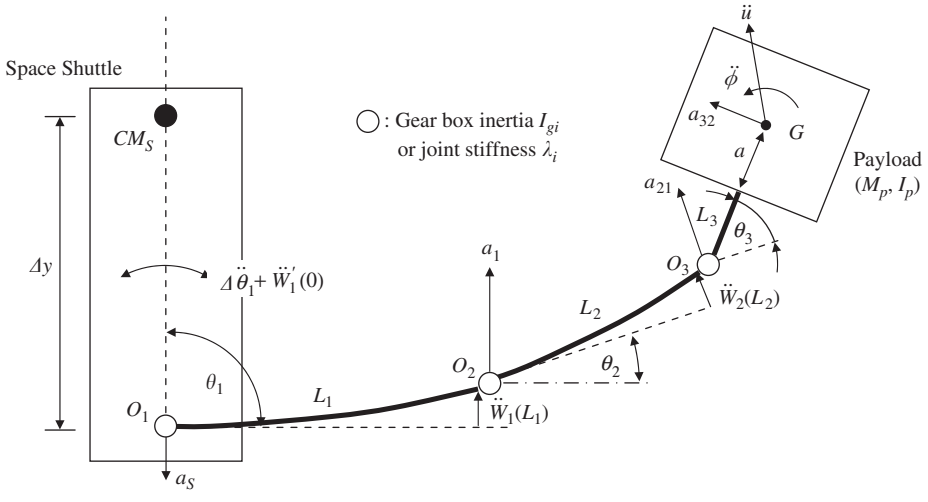

Fig. 1. Acceleration components of the SRMS with rigid payload and space shuttle.

and after collecting terms with respect to A_i, B_i, C_i and D_i, the eigenvalue equation becomes

$$\begin{bmatrix} d_{11} & d_{12} & d_{13} & d_{14} & d_{15} & d_{16} & d_{17} & d_{18} \\ d_{21} & d_{22} & d_{23} & d_{24} & d_{25} & d_{26} & d_{27} & d_{28} \\ d_{31} & d_{32} & d_{33} & d_{34} & d_{35} & d_{36} & d_{37} & d_{38} \\ d_{41} & d_{42} & d_{43} & d_{44} & d_{45} & d_{46} & d_{47} & d_{48} \\ d_{51} & d_{52} & d_{53} & d_{54} & d_{55} & d_{56} & d_{57} & d_{58} \\ d_{61} & d_{62} & d_{63} & d_{64} & d_{65} & d_{66} & d_{67} & d_{68} \\ d_{71} & d_{72} & d_{73} & d_{74} & d_{75} & d_{76} & d_{77} & d_{78} \\ d_{81} & d_{82} & d_{83} & d_{84} & d_{85} & d_{86} & d_{87} & d_{88} \end{bmatrix} \begin{bmatrix} A_1 \\ B_1 \\ C_1 \\ D_1 \\ A_2 \\ B_2 \\ C_2 \\ D_2 \end{bmatrix} = 0 \tag{3}$$

which requires numerical solution of the following determinant for the natural frequencies ω_n

$$\det[d_{ij}] = 0, \tag{4}$$

where the elements d_{ij} are given in Eq. (21). Note that in general $d_{ij} \neq d_{ji}$.

Boundary conditions: It is required to take account of the bending moment and shear force boundary conditions at joints O_1, O_2 and O_3 due to payload mass and rotary inertia for various cases of one or more joints locked in Fig. 1. The payload is idealised as a block of known mass and moment of inertia about its centre of mass G which is at distance a from the end effector. $\ddot{u}$ and $\ddot{\phi}$ are the translational and rotational accelerations of G, and O_1, O_2, O_3 are revolute joints which can be free or locked with joint stiffnesses λ_i. Δy is the distance of the Shuttle centre of mass CM_S from O_1, a_1 the acceleration of O_2 relative to O_1, a_{21} the acceleration of O_3 relative to O_2, a_{32} the acceleration of G relative to O_3 and a_S is the acceleration of the Shuttle perpendicular to L_1 at O_1.

Since the angular rotation $\Delta\theta_1 + W_1'(0)$ of Link1 at O_1 ($x_1 = 0$) due to a locked joint O_1 of torsional stiffness λ_1 and to the beam flexure is small, θ_1 can be taken as constant. $\Delta\theta_1$ allows for the modal rotation of the Shuttle, given by

$$\Delta\theta_1 = \frac{EI_1 W_1''(0)}{\lambda_1}. \tag{5}$$

For harmonic motions the transverse and rotational accelerations are, respectively,

$$\ddot{W}_i(x_i) = -\omega^2 W_i(x_i) \tag{6}$$

and

$$\ddot{W}_i'(x_i) = -\omega^2 W_i'(x_i), \tag{7}$$

where $W_i'(x_i)$ denotes the slope of link i at x_i. The bending moment and shear force boundary conditions of Link1 at O_1 ($x_1 = 0$) for a locked joint are, respectively,

$$EI_1 W_1''(0) = -I_S\omega^2(W_1'(0) - \Delta\theta_1) - \Delta y\, M_S\omega^2[W_1(0)\cos\theta_1 + \Delta y(W_1'(0) - \Delta\theta_1)] \tag{8}$$

and

$$EI_1 W_1''(0) = M_S\omega^2[W_1(0) + \Delta y(W_1'(0) - \Delta\theta_1)\cos\theta_1], \tag{9}$$

where M_S and I_S are the mass and rotary inertia of the Shuttle about its centre of mass.

To obtain the boundary conditions of Link1 at $x_1 = L_1$, we calculate the total moment about O_2 and the total force perpendicular to Link1 at O_2 due to the payload. From Fig. 1 the total angular acceleration $\ddot{\phi}$ about the payload centre of mass G is

$$\ddot{\phi} = \omega^2\left[W_1'(L_1) + W_2'(L_2) + \Delta\theta_3\right], \tag{10}$$

where $\Delta\theta_3$ is the rotation of the end effector and the payload relative to Link2 at O_3 due to the joint stiffness λ_3, given by

$$\Delta\theta_3 = \frac{EI_2 W_2''(L_2)}{\lambda_3}. \tag{11}$$

The total translatory acceleration $\ddot{u}_{1M}$ of G perpendicular to Link2 is

$$\ddot{u}_{1M} = \omega^2[W_1(L_1)\cos\theta_2 + W_2(L_2) + W_1'(L_1)[L_2 + (L_3 + a)\cos\theta_3] + [W_2'(L_2) + \Delta\theta_3](L_3 + a)\cos\theta_3], \quad (12)$$

where it is assumed that the angular deflections of the links and the end effector at the joints due the joint stiffnesses is small, so that the angles θ_2 and θ_3 of the undeformed configuration can be taken as constant.

The bending moment in Link1 at O_2 must equal the total moment about O_2 due to the various inertias, thus using Eqs. (10) and (12)

$$\begin{aligned} EI_1 W_1''(L_1) = {} & I_p\omega^2[W_1'(L_1) + W_2'(L_2) + \Delta\theta_3] + M_p\omega^2[W_2(L_2) + W_1(L_1)\cos\theta_2 + W_1'(L_1)(L_2 \\ & + (L_3 + a)\cos\theta_3) + (W_2'(L_2) + \Delta\theta_3)(L_3 + a)\cos\theta_3](L_2 + (L_3 + a)\cos\theta_3) \\ & + \int_0^{L_2} m_{b2}\omega^2[W_2 + W_1(L_1)\cos\theta_2 + W_1'(L_1)x_2]x_2\,\mathrm{d}x_2. \end{aligned} \quad (13)$$

The integrals in Eqs. (13) and (14) are the inertia moment of the distributed mass of Link2 about O_2.

The shear force of Link1 at O_2 is equal to the total force perpendicular to Link1 due to the various masses, thus if M_2 is the mass of Link2, we have

$$\begin{aligned} -EI_1 W_1'''(L_1) = {} & (M_p + M_2)\omega^2 W_1(L_1) + \int_0^{L_2} m_{b2}\omega^2(W_2 + x_2 W_1'(L_1))\cos\theta\,\mathrm{d}x_2 \\ & + M_p\omega^2(W_2'(L_2) + \Delta\theta_3)(L_3 + a)\cos(\theta_2 + \theta_3) \\ & + M_p\omega^2[W_2(L_2) + W_1'(L_1)(L_2 + (L_3 + a)\cos\theta_3)]\cos\theta_2. \end{aligned} \quad (14)$$

The boundary conditions of Link2 at $x_2 = 0$ are

$$W_2(0) = 0 \quad (15)$$

and

$$\lambda_2 W_2'(0) = EI_2 W_2''(0) \quad (16)$$

if Joint2 is locked with joint stiffness λ_2.

The boundary conditions at $x_2 = L_2$ are obtained by considering the various inertia forces at O_3. The translatory acceleration $\ddot{u}_{2M}$ of G perpendicular to the end effector is

$$\begin{aligned} \ddot{u}_{2M} = {} & \omega^2[W_1(L_1)\cos(\theta_2 + \theta_3) + (W_2'(L_2) + \Delta\theta_3)(L_3 + a)] \\ & + \omega^2[W_2(L_2) + W_1'(L_1)(L_2 + (L_3 + a)\cos\theta_3)]\cos\theta_3. \end{aligned} \quad (17)$$

Thus using Eqs. (10) and (17), moment equilibrium at O_3 gives

$$\begin{aligned} EI_2 W_2''(L_2) = {} & I_p\omega^2[W_1'(L_1) + W_2'(L_2) + \Delta\theta_3] + M_p\omega^2[W_1(L_1)\cos(\theta_2 + \theta_3) + (W_2'(L_2) + \Delta\theta_3)(L_3 + a) \\ & + \{W_2(L_2) + W_1'(L_1)(L_2 + (L_3 + a)\cos\theta_3)\}\cos\theta_3](L_3 + a). \end{aligned} \quad (18)$$

The shear force of Link2 at O_3 must be equal to all the inertia force components perpendicular to Link2 at O_3, thus

$$\begin{aligned} -EI_2 W_2'''(L_2) = {} & M_p\omega^2[W_1(L_1)\cos\theta_2 + W_2(L_2) + (W_2'(L_2) + \Delta\theta_3)(L_3 + a)\cos\theta_3 \\ & + W_1'(L_1)(L_2 + (L_3 + a)\cos\theta_3)]. \end{aligned} \quad (19)$$

Using Eq. (15) to obtain $D_2 = -B_2$ and applying the other boundary conditions we collect all terms with respect to A_1, B_1, C_1, D_1, A_2, B_2, and C_2, so that Eq. (3) reduces to the 7×7 system

$$\begin{bmatrix} d_{11} & d_{12} & d_{13} & d_{14} & d_{15} & d_{16} & d_{17} \\ d_{21} & d_{22} & d_{23} & d_{24} & d_{25} & d_{26} & d_{27} \\ d_{31} & d_{32} & d_{33} & d_{34} & d_{35} & d_{36} & d_{37} \\ d_{41} & d_{42} & d_{43} & d_{44} & d_{45} & d_{46} & d_{47} \\ d_{51} & d_{52} & d_{53} & d_{54} & d_{55} & d_{56} & d_{57} \\ d_{61} & d_{62} & d_{63} & d_{64} & d_{65} & d_{66} & d_{67} \\ d_{71} & d_{72} & d_{73} & d_{74} & d_{75} & d_{76} & d_{77} \end{bmatrix} \begin{bmatrix} A_1 \\ B_1 \\ C_1 \\ D_1 \\ A_2 \\ B_2 \\ C_2 \end{bmatrix} = 0. \tag{20}$$

Neglecting the small integral terms in Eqs. (13) and (14) and using $C_1 = \cos(k_1 L_1)$, $S_1 = \sin(k_1 L_1)$, $Ch_1 = \cosh(k_1 L_1)$, $Sh_1 = \sinh(k_1 L_1)$, $C_2 = \cos(k_2 L_2)$, $S_2 = \sin(k_2 L_2)$, $Ch_2 = \cosh(k_2 L_2)$, $Sh_2 = \sinh(k_2 L_2)$, the elements d_{ij} in Eq. (20) are

$$\begin{aligned}
d_{11} &= d_{13} = k_1(I_S + \Delta y^2 M_S)\omega^2, \\
d_{12} &= EI_1 k_1^2\left(-1 + \frac{(I_S + \Delta y^2 M_S)\omega^2}{\lambda_1}\right) + \omega^2 \Delta y M_S \cos\theta_1, \\
d_{14} &= EI_1 k_1^2\left(1 - \frac{(I_S + \Delta y^2 M_S)\omega^2}{\lambda_1}\right) + \omega^2 \Delta y M_S \cos\theta_1, \\
d_{15} &= d_{16} = d_{17} = 0, \\
d_{21} &= EI_1 k_1^3 + \omega^2 k_1 \Delta y M_S \cos\theta_1, \\
d_{22} &= \omega^2 M_S\left(1 + \frac{k_1^2 \Delta y EI_1 \cos\theta_1}{\lambda_1}\right), \\
d_{23} &= -EI_1 k_1^3 + \omega^2 k_1 \Delta y M_S \cos\theta_1, \\
d_{24} &= \omega^2 M_S\left(1 - \frac{k_1^2 \Delta y EI_1 \cos\theta_1}{\lambda_1}\right),
\end{aligned}$$

$$\begin{aligned}
d_{25} &= d_{26} = d_{27} = 0, \\
d_{31} &= k_1(I_p + M_p(L_2 + (a + L_3)\cos\theta_3)^2)\omega^2 C_1 + S_1(EI_1 k_1^2 + M_p(L_2 + (a + L_3)\cos\theta_3)\omega^2 \cos\theta_2), \\
d_{32} &= C_1(M_p\omega^2 \cos\theta_2(L_2 + (a + L_3)\cos\theta_3) + EI_1 k_1^2) - \omega^2 I_p k_1 S_1 - \omega^2 M_p k_1(L_2 + (a + L_3)\cos\theta_3)^2 S_1, \\
d_{33} &= k_1(I_p + M_p(L_2 + (a + L_3)\cos\theta_3)^2)\omega^2 Ch_1 - Sh_1(EI_1 k_1^2 - M_p(L_2 + (a + L_3)\cos\theta_3)\omega^2 \cos\theta_2), \\
d_{34} &= Ch_1(M_p\omega^2 \cos\theta_2(L_2 + (a + L_3)\cos\theta_3) - EI_1 k_1^2) + \omega^2 I_p k_1 Sh_1 + \omega^2 M_p k_1(L_2 + (a + L_3)\cos\theta_3)^2 Sh_1,
\end{aligned}$$

$$\begin{aligned}
d_{35} &= \omega^2(M_p(L_2 + (a + L_3)\cos\theta_3)S_2 + I_p k_2 C_2) \\
&\quad + \omega^2\left(-\frac{I_p k_2^2 EI_2 S_2}{\lambda_3} + k_2(a + L_3)M_p \cos\theta_3(L_2 + (a + L_3)\cos\theta_3)\left(C_2 - \frac{EI_2 k_2 S_2}{\lambda_3}\right)\right), \\
d_{36} &= \omega^2(M_p(L_2 + (a + L_3)\cos\theta_3)(C_2 - Ch_2)) + \omega^2\left(-I_p k_2\left(S_2 + Sh_2 + \frac{EI_2 k_2(C_2 + Ch_2)}{\lambda_3}\right)\right), \\
&\quad - \omega^2\left(M_p k_2 \cos\theta_3(a + L_3)(L_2 + (a + L_3)\cos\theta_3)\left(S_2 + Sh_2 + \frac{EI_2 k_2(C_2 + Ch_2)}{\lambda_3}\right)\right),
\end{aligned}$$

$$d_{37} = \omega^2(M_p(L_2 + (a+L_3)\cos\theta_3)Sh_2 + I_p k_2 Ch_2) + \omega^2\left(\frac{I_p k_2^2 EI_2 Sh_2}{\lambda_3} + k_2(a+L_3)M_p\cos\theta_3(L_2+(a+L_3)\cos\theta_3)\left(Ch_2 + \frac{EI_2 k_2 Sh_2}{\lambda_3}\right)\right),$$

$$d_{41} = k_1 C_1(-EI_1 k_1^2 + M_p\omega^2\cos\theta_2(L_2+(a+L_3)\cos\theta_3)) + (M_p+M_2)\omega^2 S_1,$$

$$d_{42} = \omega^2(M_p+M_2)C_1 + EI_1 k_1^3 S_1 - k_1 M_p\omega^2\cos\theta_2(L_2+(a+L_3)\cos\theta_3)S_1,$$

$$d_{43} = k_1 Ch_1(EI_1 k_1^2 + M_p\omega^2\cos\theta_2(L_2+(a+L_3)\cos\theta_3)) + (M_p+M_2)\omega^2 Sh_1,$$

$$d_{44} = \omega^2(M_p+M_2)Ch_1 + EI_1 k_1^3 Sh_1 + k_1 M_p\omega^2\cos\theta_2(L_2+(a+L_3)\cos\theta_3)Sh_1,$$

$$d_{45} = \frac{\omega^2}{k_2\lambda_3}(-k_2^2(a+L_3)M_p\cos(\theta_2+\theta_3)(-\lambda_3 C_2 + EI_2 k_2 S_2)) + \omega^2\cos\theta_2 M_p S_2,$$

$$d_{46} = \omega^2 M_p\cos\theta_2(C_2 - Ch_2) - \omega^2\left(k_2(a+L_3)M_p\cos(\theta_2+\theta_3)\left(S_2 + Sh_2 + EI_2 k_2\frac{C_2+Ch_2}{\lambda_3}\right)\right),$$

$$d_{47} = \frac{\omega^2}{k_2\lambda_3}(k_2^2(a+L_3)M_p\cos(\theta_2+\theta_3)(\lambda_3 Ch_2 + EI_2 k_2 Sh_2)) + \omega^2\cos\theta_2 M_p Sh_2,$$

$$d_{51} = d_{52} = d_{53} = d_{54} = 0,$$

$$d_{55} = d_{57} = k_2\lambda_2,$$

$$d_{56} = 2EI_2 k_2^2,$$

$$d_{61} = \omega^2(I_p k_1 C_1 + k_1(a+L_3)M_p C_1\cos\theta_3(L_2+(a+L_3)\cos\theta_3)) + \omega^2((a+L_3)M_p C_1\cos(\theta_2+\theta_3)S_1),$$

$$d_{62} = \omega^2((a+L_3)M_p C_1\cos(\theta_2+\theta_3) - I_p k_1 S_1) - \omega^2 k_1(a+L_3)M_p\cos\theta_3(L_2+(a+L_3)\cos\theta_3)S_1,$$

$$d_{63} = \omega^2(I_p k_1 Ch_1 + k_1(a+L_3)M_p Ch_1\cos\theta_3(L_2+(a+L_3)\cos\theta_3)) + \omega^2((a+L_3)M_p C_1\cos(\theta_2+\theta_3)Sh_1),$$

$$d_{64} = \omega^2((a+L_3)M_p C_1\cos(\theta_2+\theta_3) + I_p k_1 Sh_1) + \omega^2 k_1(a+L_3)M_p\cos\theta_3(L_2+(a+L_3)\cos\theta_3)Sh_1,$$

$$d_{65} = EI_2 k_2^2 S_2 + \omega^2\left((a+L_3)M_p\cos\theta_3 S_2 + I_p k_2\left(C_2 - EI_2 k_2\frac{S_2}{\lambda_3}\right)\right) + k_2(a+L_3)^2 M_p\omega^2\left(C_2 - EI_2 k_2\frac{S_2}{\lambda_3}\right),$$

$$d_{66} = EI_2 k_2^2(C_2+Ch_2) + \omega^2(a+L_3)M_p\cos\theta_3(C_2-Ch_2) + \omega^2 I_p k_2\left(S_2 + Sh_2 + EI_2 k_2\frac{C_2+Ch_2}{\lambda_3}\right) + k_2(a+L_3)^2 M_p\omega^2\left(S_2 + Sh_2 + EI_2 k_2\frac{C_2+Ch_2}{\lambda_3}\right)$$

$$d_{67} = \omega^2\left((a+L_3)M_p\cos\theta_3 Sh_2 + I_p k_2\left(Ch_2 + EI_2 k_2\frac{Sh_2}{\lambda_3}\right)\right) - EI_2 k_2^2 Sh_2 + k_2(a+L_3)^2 M_p\omega^2\left(Ch_2 + EI_2 k_2\frac{Sh_2}{\lambda_3}\right),$$

$$d_{71} = M_p\omega^2(k_1 C_1(L_2+(a+L_3)\cos\theta_3) + \cos\theta_2 S_1),$$

$$d_{72} = M_p\omega^2(-k_1(L_2+(a+L_3)\cos\theta_3)S_1 + \cos\theta_2 C_1),$$

$$d_{73} = M_p\omega^2(k_1 C_1(L_2+(a+L_3)\cos\theta_3) + \cos\theta_2 Sh_1),$$

$$d_{74} = M_p\omega^2(k_1(L_2+(a+L_3)\cos\theta_3)Sh_1 + \cos\theta_2 Ch_1),$$

$$d_{75} = -EI_2 k_2^3 C_2 + M_p\omega^2\left(S_2 + k_2(a+L_3)\cos\theta_3\left(C_2 - EI_2 k_2\frac{S_2}{\lambda_3}\right)\right),$$

$$d_{76} = EI_2k_2^3(S_2 - Sh_2) + M_p\omega^2\left(C_2 - Ch_2 - k_2(a + L_3)\cos\theta_3\left(S_2 + Sh_2 + EI_2k_2\frac{C_2 + Ch_2}{\lambda_3}\right)\right),$$

$$d_{77} = EI_2k_2^3Ch_2 + M_p\omega^2\left(Sh_2 + k_2(a + L_3)\cos\theta_3\left(Ch_2 + EI_2k_2\frac{Sh_2}{\lambda_3}\right)\right). \quad (21)$$

For an unlocked joint, λ_1 is set to a very small value (zero is not allowed, since it appears in denominators), and Eq. (8) becomes

$$-EI_1W_1''(0) = I_{g1}\omega^2W_1'(0). \quad (22)$$

Then the elements d_{11}, d_{12}, d_{13} and d_{14} in Eq. (21) become

$$d_{11} = d_{13} = I_{g1}k_1\omega^2,$$
$$d_{14} = -d_{12} = EI_1k_1^2. \quad (23)$$

In Eqs. (22) and (23) I_{g1} denotes the effective moment of inertia at the output side of the gearbox at O_1 due to the backdriveability of the high ratio gear trains. Similarly, I_{g2} is the effective moment of inertia at the output side of the gearbox at O_2. The effective moment of inertia of the end effector joint O_3 can be included in the payload properties but is negligibly small.

For an unlocked Joint2, λ_2 is set to a very small value, and Eq. (16) becomes

$$-EI_2W_2''(0) = I_{g2}\omega^2W_2'(0) \quad (24)$$

and the elements d_{55} and d_{57} in Eq. (21) are

$$d_{55} = d_{57} = -I_{g2}k_2\omega^2. \quad (25)$$

Note that deriving the above matrix elements by hand is very tedious and prone to error. For complex systems it is therefore recommended to use software that can handle symbolic calculations to derive the matrix elements.

3. Mode shape determination

Using Eq. (4) the computed natural frequency ω_n can be re-inserted into Eqs. (3) or (20) respectively, where all the matrix elements are now known. Taking for example $A_1 = 1$ and deleting any one of the seven equations (20) or, in the general case, of the eight equations (3), the remaining equations can be solved for the remaining parameters B_1, C_1, etc.

Thus knowing all variables, the parameters A_1, B_1, … are inserted into Eq. (1), together with the known ω_n, which finally yields the two mode shapes $W_i(x)$ for each of the two flexible links for the natural frequency ω_n.

It is noted that although the mode shapes are computed for one configuration or moment in time, it will be shown in Section 6 that for the relevant cases with non-negligible elastic deflections, the mode shapes of the two flexible links remain essentially the same throughout a manoeuvre and can thus be used also for non-static dynamic response analyses with changing SRMS configurations, as long as the joint configuration remains the same.

4. Orthogonality of normal modes

We apply the method presented in Ref. [18] for finding the orthogonality condition of an arbitrary system of interconnected Euler–Bernoulli beams subject to arbitrary boundary conditions. Thus for the present system and for the case Joint1 locked and Joint2 locked, using Eqs. (8), (9), (11), (15), (16), (18) and (19), and letting $W_{n1}(x)$ and $W_{n2}(x)$ be the nth mode shape for Beam1 and Beam2, respectively, the orthogonality condition is

given as

$$\begin{aligned}
&\int_0^{L_1} m_{b1} W_{n1}(x_1) W_{m1}(x_1)\,\mathrm{d}x_1 + \int_0^{L_2} m_{b2} W_{n2}(x_2) W_{m2}(x_2)\,\mathrm{d}x_2 + I_S(W'_{n1}(0)W'_{m1}(0) - \Delta\theta_1)\\
&+ \Delta y\, M_S[W_{n1}(0)W_{m1}(0)\cos\theta_1 + \Delta y(W'_{n1}(0)W'_{m1}(0) - \Delta\theta_1)] + M_S[W_{n1}(0)W_{m1}(0)\\
&+ \Delta y(W'_{n1}(0)W'_{m1}(0) - \Delta\theta_1)\cos\theta_1] + I_p[W'_{n1}(L_1)W'_{m1}(L_1) + W'_{n2}(L_2)W'_{m2}(L_2) + \Delta\theta_3]\\
&+ M_p[W_{n2}(L_2)W_{m2}(L_2) + W_{n1}(L_1)W_{m1}(L_1)\cos\theta_2 + W'_{n1}(L_1)W'_{m1}(L_1)(L_2 + (L_3 + a)\cos\theta_3)\\
&+ W'_{n2}(L_2)W'_{m2}(L_2) + \Delta\theta_3)(L_3 + a)\cos\theta_3](L_2 + (L_3 + a)\cos\theta_3)\\
&+ \int_0^{L_2} m_{b2}[W_{n2}(x_2)W_{m2}(x_2) + W_{n1}(L_1)W_{m1}(L_1)\cos\theta_2 + W'_{n1}(L_1)W'_{m1}(L_1)x_2]x_2\,\mathrm{d}x_2\\
&+ (M_p + M_2)W_{n1}(L_1)W_{m1}(L_1) + \int_0^{L_2} m_{b2}[W_{n2}(x_2)W_{m2}(x_2) + x_2 W'_{n1}(L_1)W'_{m1}(L_1)]\cos\theta\,\mathrm{d}x_2\\
&+ M_p(W'_{n2}(L_2)W'_{m2}(L_2) + \Delta\theta_3)(L_3 + a)\cos(\theta_2 + \theta_3) + M_p[W_{n2}(L_2)W_{m2}(L_2)\\
&+ W'_{n1}(L_1)W'_{m1}(L_1)(L_2 + (L_3 + a)\cos\theta_3)]\cos\theta_2\\
&+ \lambda_2 W'_{n2}(0)W'_{m2}(0) + I_p\omega^2[W'_{n1}(L_1)W'_{m1}(L_1) + W'_{n2}(L_2)W'_{m2}(L_2) + \Delta\theta_3]\\
&+ M_p[W_{n1}(L_1)W_{m1}(L_1)\cos(\theta_2 + \theta_3) + (W'_{n2}(L_2)W'_{m2}(L_2) + \Delta\theta_3)(L_3 + a)\\
&\{W_{n2}(L_2)W_{m2}(L_2) + W'_{n1}(L_1)W'_{m1}(L_1)(L_2 + (L_3 + a)\cos\theta_3)\}\cos\theta_3](L_3 + a)\\
&+ M_p[W_{n1}(L_1)W_{m1}(L_1)\cos\theta_2 + W_{n2}(L_2)W_{m2}(L_2) + (W'_{n2}(L_2)W'_{m2}(L_2) + \Delta\theta_3)(L_3 + a)\cos\theta_3\\
&+ W'_{n1}(L_1)W'_{m1}(L_1)(L_2 + (L_3 + a)\cos\theta_3)] = 0
\end{aligned} \tag{26}$$

for any $m \neq n$. As shown in Ref. [18], the orthogonality condition is derived by taking the kinetic energy expressed by all boundary conditions, independent of its sign, adding up all terms, waiving the ω_n and replacing $W_1(x)$ with the product of two mode shapes $W_{n1}(x)$ and $W_{m1}(x)$ (similar for $W_2(x)$).

The result is identical to the generalised mass expression obtained with the first term of Lagrange's equation

$$\frac{\mathrm{d}}{\mathrm{d}t}\left(\frac{\partial T}{\partial \dot{q}_i(t)}\right) + \frac{\partial V}{\partial q_i(t)} = 0, \tag{27}$$

where T is the system kinetic energy and V the elastic strain energy of the links. Due to this fact, the off-diagonal elements of the mass matrix $\mathbf{M}$ as obtained with the first term of Eq. (27) or as obtained with the left-hand side of Eq. (26) for $m \neq n$ are an indicator for the precision of the computations and a measure for the orthogonality of the eigenmodes. Knowing also the system stiffness matrix $\mathbf{K}$ obtained with the second term of Eq. (27), natural frequencies and mode shapes for the system can be computed with

$$\left|\mathbf{K} - \omega^2\mathbf{M}\right| = 0. \tag{28}$$

5. Numerical results for natural frequencies and mode shapes

It is seen that the present system can have eight different joint configurations depending on which of the three joints are locked or free. Due to the large number of possibilities even for fixed joint angle steps of say 30°, we only consider the straight RMS perpendicular to the Shuttle axis ($\theta_1 = 90^\circ$, $\theta_2 = \theta_3 = 0^\circ$) for each joint configuration, which will give the very lowest frequency possible for the case all joints locked. Table 1 compares the fundamental frequency ω_1 for a free base (Shuttle) to that for a fixed base, which could for example be true for the case of an attitude controlled Shuttle or a Shuttle docked to a much larger body such as the International Space Station. The joint configurations are indicated using 1 for a locked joint and 0 for a free joint. Thus 1-0-1 for example means Joint1 and Joint3 locked and Joint2 unlocked.

The manipulator properties are chosen identical to the SRMS [3], which are given as $L_1 = 6.37\,\mathrm{m}$, $L_2 = 7.05\,\mathrm{m}$, $L_3 = 1.88\,\mathrm{m}$, $m_{b1} = 3.9\,\mathrm{kg/m}$, $m_{b2} = 3.4\,\mathrm{kg/m}$, $EI_1 = 3.9786 \times 10^6\,\mathrm{N\,m^2}$ and $EI_2 = 2.334 \times$

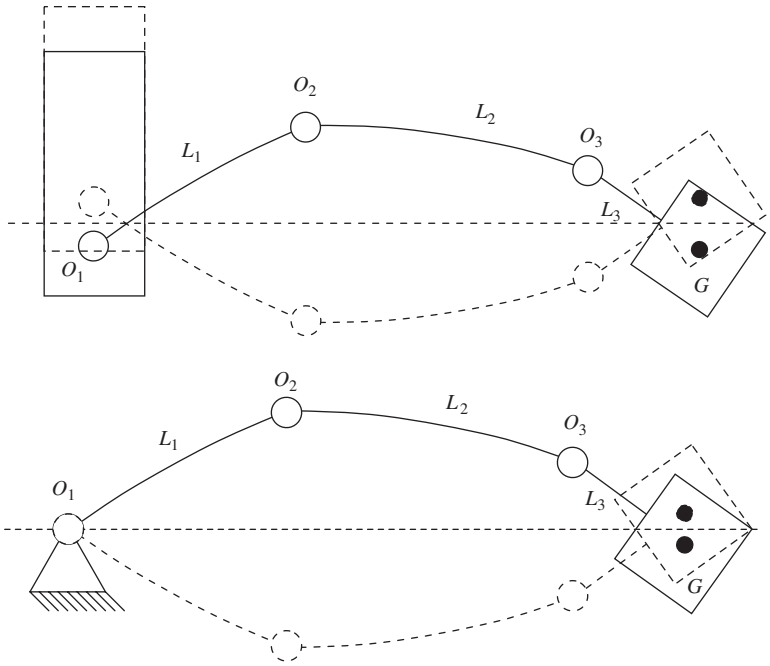

Figs. 2 and 3. First mode shape for free and fixed base (joint configuration 0-1-1).

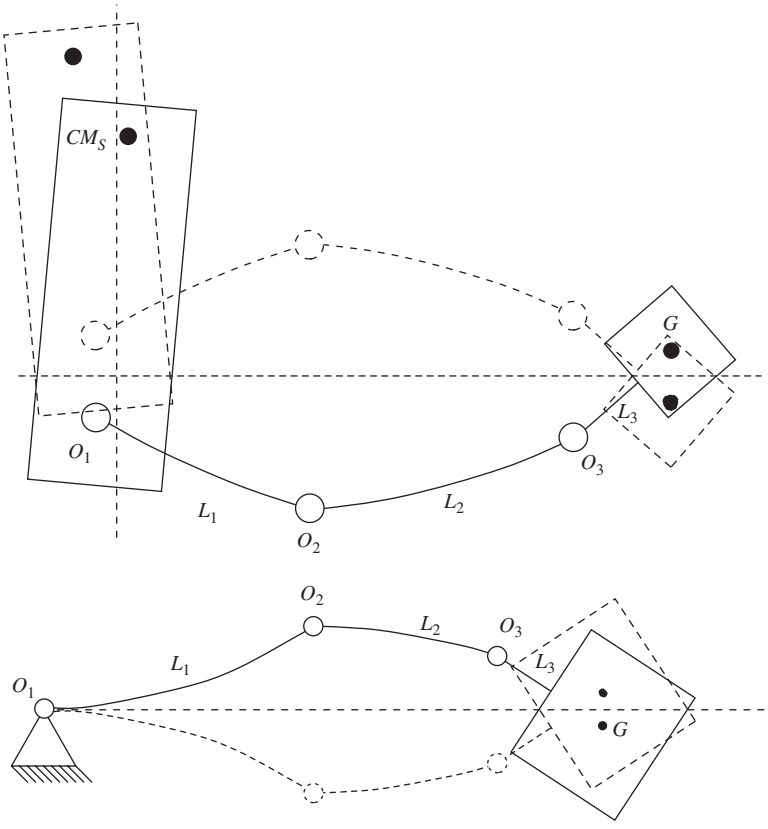

Figs. 4 and 5. First mode shape for free and fixed base (1-0-1).

Table 1
Fundamental frequency ω_1 (rad/s) of double flexible link system with end effector and unconstrained shuttle

Joint config.	Free base	Fixed base
0-0-0	30.94	34.04
0-0-1	5.11	6.04
0-1-0	18.37	22.44
1-0-0	10.59	13.33
0-1-1	0.84	0.83
1-0-1	1.05	1.02
1-1-0	0.46	0.40
1-1-1	0.31	0.17

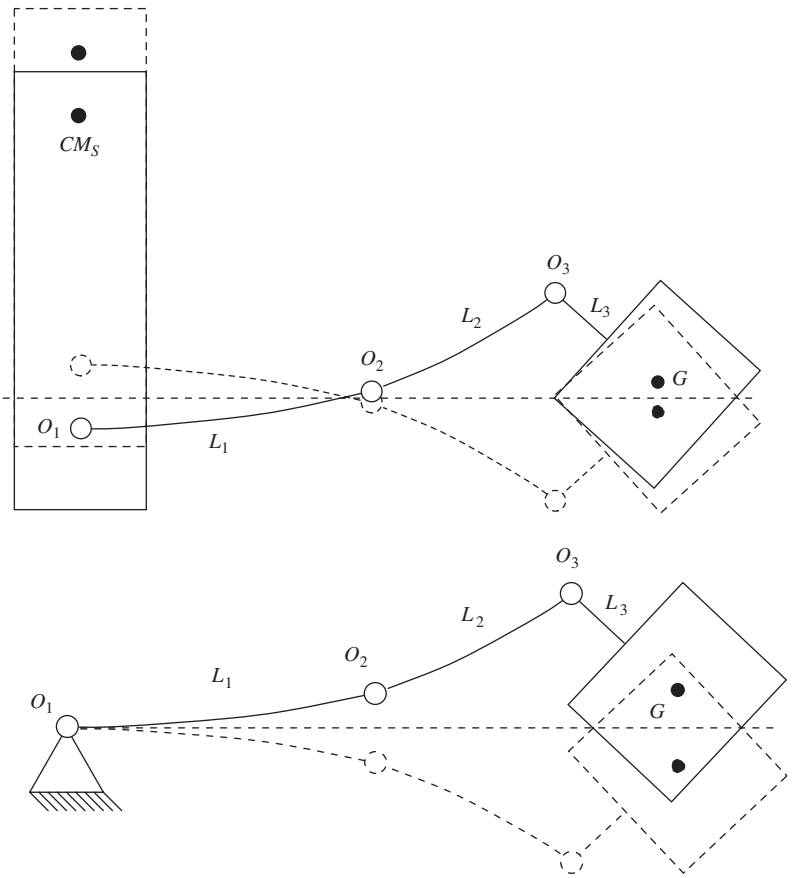

Fig. 6 and 7. First mode shape for free and fixed base (1-1-0).

$10^6\,\mathrm{N\,m^2}$. The joints properties are $\lambda_1 = 10^6\,\mathrm{N\,m/rad}$ or $I_{g1} = 1188\,\mathrm{kg\,m^2}$, $\lambda_2 = 10^6\,\mathrm{N\,m/rad}$ or $I_{g1} = 556\,\mathrm{kg\,m^2}$ and $\lambda_3 = 2.4 \times 10^5\,\mathrm{N\,m/rad}$ or $\lambda_3 = 10^{-3}\,\mathrm{N\,m/rad}$, respectively, if the actual joint is locked or unlocked.

The payload is chosen to be maximum, thus $M_p = 30{,}000\,\mathrm{kg}$, $I_p = 400{,}000\,\mathrm{kg\,m^2}$ and $a = 2\,\mathrm{m}$, and the Shuttle properties are estimated with the available literature as $\Delta y = 14\,\mathrm{m}$, $M_S = 7 \times 10^5\,\mathrm{kg}$ and $I_S = 10^6\,\mathrm{kg\,m^2}$.

Figs. 2–5 show the mode shapes corresponding to the fundamental natural frequencies in Table 1 for the joint configurations with at least two joints locked (Figs. 6–9).

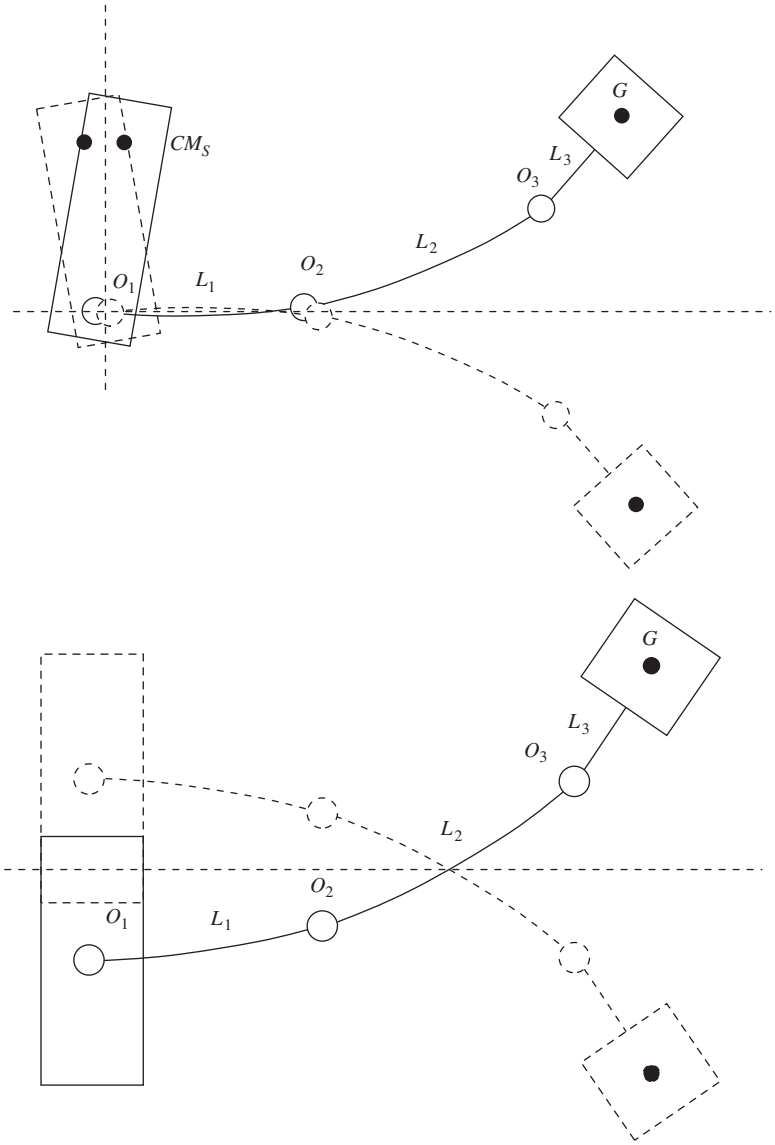

Figs. 8 and 9. First mode shape for free and linearly translating base for (1-1-1).

Dynamic simulations carried out in Ref. [20] and using the exact eigenmodes computed with the determinant method given here show that the results differ significantly from those of other researchers. It is believed that this difference is due to two facts:

(1) usually, a standard multimode expansion using assumed mode shapes is applied to account for the link flexibility; however, no justification and no proof of convergence is normally given along with the results;
(2) many of the available papers do not account for the exact boundary conditions of the flexible links when the joint brakes are unlocked; in this case the boundary conditions of the flexible links are essentially a pin joint due to joint backdriveability, even in the presence of the large rotary inertia due to the effective rotor inertia at the output side of the high ratio gear train; pinned boundary conditions however make for much smaller elastic deflections than cantilever beam boundary conditions, as normally assumed.

Due to these facts it is furthermore assumed that since under normal conditions the elastic deflections are very small in reality, no active damping system need to be installed on space robotic systems comparable to the SRMS. This is also in contrast to the results of a number of papers that propose a wide range of active and passive damping systems for the SRMS.

6. Optimisation of numerical simulations

6.1. Using exact mode shapes

Ref. [20] shows that for dynamic response analyses, only the fundamental mode computed with the above method has to be taken into account for elastic modeling, covering about 98% or more of the total elastic deflection in all simulations [19] shows that in order to approximate the exact fundamental mode shape, a standard multimode expansion with assumed mode shapes as normally used by other researchers would need a relatively large number of modes to converge to an acceptable level, thus dramatically increasing computation time.

6.2. Mode shape simplification

For dynamic response analyses, the exact analytical mode shapes expressed by Eq. (1) may be undesirable, containing complex trigonometric and hyperbolic functions and therefore being unsatisfactory for numerical simulations of flexible robot systems.

A polynomial approximation of the exact mode shape functions in Eq. (1) can be obtained by a standard interpolation fit in the form $W_{\text{app}}(x) = \sum_{n=1}^{N} a_n x^n$. Prior to any computations however it should be ensured that the approximate polynomials deviate only with a maximum relative magnitude of say, 10^{-3} from the original functions. These mode shapes are then used in Eq. (27).

6.3. Tangent frame formulation

Although the mode shapes are computed for one configuration or moment in time, all formulations of the boundary conditions of the elastic beams for mode shape and eigenfrequency determination use a tangent frame. Thus the kinematics of any body within the chain of bodies of the dynamical system are always formulated relative to the previous body in the chain.

The advantage of using the tangent frame formulation is the following. Since the kinematics of any body are expressed relative to the previous body, a motion for example of the end effector about O_3 changes nothing in the formulation of all previous bodies in the chain, that is of the whole rest of the system.

Another example is the step from a fixed RMS base to a free base (and vice versa). If the tangent frame formulation is used to set up the boundary conditions for the flexible links for say, the fixed RMS base case, only the boundary conditions of Link1 at $x_1 = 0$ has to be modified to allow for a free floating Shuttle, whereas all the other equations representing the other boundary conditions could remain unchanged.

Since the mode shapes of the two flexible links are always computed for only one moment in time, they could basically not be used for dynamic simulations with time-varying states. Using the tangent frame formulation however to set up the equations of motion, simulations can be carried out always using the same mode shapes for the whole simulation, provided that in reality the mode shapes do not change significantly with a changing configuration. Table 2 is given for a proof.

Table 2
First non-zero frequency ω_{det} of determinant for fixed base SRMS and ω_{Lag} of Eq. (28) for one fixed set of mode shapes

θ_2 (deg)	0	30	60	90
ω_{det} (rad/s)	1.02	0.98	0.82	0.73
ω_{Lag} (rad/s)	1.02	0.98	0.82	0.73

Table 3
First non-zero frequency ω_{det} of determinant for Section 5 system and ω_{Lag} of Eq. (28) for one fixed set of mode shapes

θ_3 (deg)	0	30	60	90
ω_{det} (rad/s)	0.40	0.33	0.27	0.27
ω_{Lag} (rad/s)	0.40	0.34	0.29	0.27

Table 2 gives the first non-zero natural frequencies for the data set defined in Section 5 for the SRMS with fixed base (for which the joint angle θ_1 is irrelevant) for various joint angles θ_2, while $\theta_3 = 0^\circ$. These exact natural frequencies ω_{det} are computed with the determinant method outlined before. The ω_{det} are compared to the first non-zero natural frequencies computed with Eq. (28) when for the flexible Link1 and Link2 only the fundamental mode shape computed with the determinant method for the configuration $\theta_2 = \theta_3 = 0^\circ$ is inserted and θ_2 then varied. These latter frequencies computed with Lagrange's method are denoted ω_{Lag}.

Table 2 clearly proves the aforementioned benefit of using the tangent frame, since the mode shapes remain practically constant with changing θ_2. Thus only one set of mode shapes is sufficient for dynamic analyses with time varying configurations.

Table 3 makes the same comparison for the configuration, Joint1 and Joint2 locked and Joint3 unlocked. Again, for Lagrange's equation the mode shapes of the flexible links were computed for $\theta_2 = \theta_3 = 0^\circ$. Like Table 2, Table 3 proves the validity of the tangent frame formulation.

One side effect when using the tangent frame formulation must however be noted. Since a modal decomposition due to time varying configurations is not possible, the system obtained with Lagrange's Eq. (27) will have more than only the one natural frequency for which the inserted mode shapes were computed. Consider the following example. One mode shape for each flexible link for the configuration of all joints locked is computed with the determinant method and inserted into equations of motion obtained with the tangent frame formulation. Now if the system has a fixed base, Eq. (27) will give three natural frequencies and thus three mode shapes due to three degrees of freedom: a rigid body rotation of the end effector, a flexible motion of Link2 and a flexible motion of Link1. Originally however, the mode shapes belonged to only one system mode. For the relevant cases of non-negligible elastic deflections, the application of the presented method shows that the influence of these "artificial" additional mode shapes is irrelevant here.

6.4. Mode shape modification for dynamic simulations

For dynamic simulations using the tangent frame formulation the kinematics of any body within the chain of bodies of the system are always formulated relative to the previous body in the chain. Therefore a correction has to be made to the non-rigid mode shapes of the first flexible link due to the following reason. The functions $W_{1,i}(x_1)$ in their present form contain also the rotatory and translatory motion of the Shuttle in the actual vibration mode. But for further use in dynamic response analyses, the functions must only represent the deflection of Link1 relative to the Shuttle. Therefore, since all deflections are linearised, the corrected mode shape for Link1 is obtained by letting $W_{1,i\,\mathrm{correct}}(x_1) = W_{1,i}(x_1) - W_{1,i}(0) + \Delta\theta_1 x_1$, where $\Delta\theta_1$ is the modal rotation of the Shuttle given by Eq. (5) and is known after applying the aforementioned method of re-inserting a known ω_n into the respective equation systems to obtain the mode shapes. For an unlocked Joint1, the $\Delta\theta_1$ term in the above equation is waived, since in that case Shuttle rotational motions are not transmitted through Joint1.

7. Limits in numerical accuracy using the determinant method

It is found that due to the great complexity of the determinant equation (4) for the present case (the determinant expression is about 50 pages long, including hundreds of the trigonometric and hyperbolic functions and all kinds of products), frequencies in excess of about 5 rad/s may not be accurate, but as has been shown in Ref. [20], frequencies of that order are associated with negligibly small elastic deflections.

Table 4
Mass matrix **M** for double flexible link system with free base (shuttle) and data set of Section 5, using three exact mode shapes

1	10^{-5}	10^{-3}
10^{-5}	1	10^{-2}
10^{-3}	10^{-2}	1

It is known that the magnitude of the off-diagonal elements in the mass matrix **M** in Eqs. (27) or (28) or the left-hand side of Eq. (26) for $m \neq n$ are an indicator for the numerical accuracy when using exact mode shapes. Table 4 gives the mass matrix **M** for the double flexible link system with free base for the data set introduced in Section 5.

From the above table it can be seen that the numerical accuracy can rapidly decrease with an increasing number of mode shapes in dynamical simulations. However, only the fundamental mode was found to be relevant for dynamic response analyses in Ref. [20] when the focus is on the magnitude of elastic deformations. Also, Ref. [18] shows that it is possible to smooth out the inaccuracies by computing the eigenvectors of the systems with Eq. (28), so as to make the mode shapes more orthogonal.

For simpler systems than the one proposed here, for example a system as analysed in Ref. [16], the application of the method developed in Ref. [18] shows that the off-diagonal elements of the mass matrix are of the order of 10^{-7}, even for 10 and more modes shapes, and this is believed to be a limit in numerical accuray in general, not only for the proposed method.

8. Summary

This paper gives an exact analytical solution for the natural frequencies and mode shapes of a triply articulated planar manipulator system with two long flexible links and one short, rigid end effector, similar to the shuttle remote manipulator system (SRMS). It is an application of Wiedemann [18] and an extension of Wiedemann and Kirk [20] in that it gives the orthogonality condition of the mode shapes and considers optimisation of numerical simulations and limits in numerical accuracy when using the proposed method.

The present paper gives numerical results for the exact fundamental natural frequency and mode shape of a space robotic system similar to the SRMS for various configurations of joints free and fixed and included angles θ_1, θ_2 and θ_3. It is shown how numerical dynamic simulations can be optimised in terms of computation time and accuracy of the results.

The limits in numerical accuracy when using the proposed method to find eigenmodes of flexible robotic systems are addressed, and referring to results of Wiedemann and Kirk [20] these are shown to be unproblematic since the fundamental mode covers about 98% of the total elastic deflection excited by manoeuvers of the SRMS.

The paper applies the exact boundary conditions when formulating the links equations of motion, thus revealing that when the joints are unlocked, the links are essentially pinned, and not clamped as assumed in other papers. Thus with essentially pinned flexible links, the elastic deflections are small compared to those computed in other papers when assuming clamped flexible links. Since NASA has, to the authors' knowledge, not introduced active damping control of the SRMS so far, it is believed that the results given in this paper and in Ref. [20] are therefore closer to reality than those of other publications.

References

[1] D.M. Gossain, E. Quittner, S.S. Sachdev, Analysis and design of the shuttle remote manipulator system mechanical arm for launch dynamic environment, *Shock and Vibration Bulletin* (1980).

[2] D.R. Dunbar, A.R. Robertson, Graphite/epoxy booms for the shuttle remote manipulator, *Proceedings of the Second International Conference on Composite Materials*, April 16–20, 1978, Toronto, Canada.

[3] D.J. Hedley, *Design Characteristic and Design Feature Analysis of the Shuttle Remote Manipulator Arm*, Society of Automotive Engineers, 1987.

[4] J.A. Hunter, T.H. Ussher, D.M. Gossain, *Structural Dynamic Design of the Shuttle Remote Manipulator System*, AIAA, New York.

[5] O. Prakash II, N.J. Adams, B.D. Appleby, Multivariable control of the space shuttle remote manipulator system, *Proceedings of the AIAA Guidance, Navigation and Control Conference*, August 12–14, Vol. 3, New Orleans, LA, 1991.
[6] P. Kumar, P. Truss, C.G. Wagner-Bartak, System design features of the space shuttle remote manipulator, *Proceedings of the Fifth World Congress on Theory of Machines and Mechanisms*, July 1979, Montreal, Canada.
[7] R. Ravindran, K.H. Doetsch, *Design Aspects of the Shuttle Remote Manipulator Control*, American Institute of Aeronautics and Astronautics, 1982.
[8] Y. Chen, L. Meirovitch, Control of a flexible space robot executing a docking maneuver, *Journal of Guidance and Control* 18 (4) (1995).
[9] M.A. Scott, M.G. Gilbert, M.E. Demeo, Active vibration damping of the space shuttle remote manipulator system, *AIAA Guidance, Navigation and Control Conference*, New Orleans, August 12–14, 1991, pp. 194–204.
[10] E.C. Wu, J.C. Wang, J.T. Chladek, Fault-tolerant joint development for the space shuttle remote manipulator system: analysis and experiment, *IEEE Transactions on Robotics and Automation* 9 (5) (1993).
[11] R. Ravindran, P.K. Nguyen, Control of the shuttle remote manipulator, *Proceedings of the Sixth Canadian Congress of Applied Mechanics*, Vancouver, May 29–June 3, 1977.
[12] J.A. Hunter, T.H. Ussher, D.M. Gossain, Structural dynamics considerations of the shuttle remote manipulator system, *Proceedings of the AIAA 23rd Structures, Structural Dynamics and Materials Conference*, May 1982, paper 82-0762, pp. 499–505.
[13] X. Cyril, A.K. Misra, M. Ingham, G.J. Jaar, Postcapture dynamics of a spacecraft-manipulator-payload system, *Journal of Guidance, Control and Dynamics* 23 (1) (2000).
[14] S.H. Farghaly, Bending vibrations of an axially loaded cantilever beam with an elastically mounted end mass of finite length, *Journal of Sound and Vibration* 156 (2) (1992).
[15] D. Li, J.W. Zu, A.A. Goldenberg, Dynamic modeling and mode analysis of flexible-link, flexible-joint robots, *Mechanic Machines Theory* 33 (7) (1998) 1031–1044.
[16] C.L. Kirk, S.M. Wiedemann, Natural frequencies and mode shapes of a free–free beam with large end masses, *Journal of Sound and Vibration* 254 (5) (2002) 939–949.
[17] M.K. Kwak, L. Meirovitch, New approach to the manoeuvering and control of flexible multibody systems, *Journal of Guidance, Control and Dynamics* 15 (6) (1992) 1342–1353.
[18] S.M. Wiedemann, Natural frequencies and mode shapes of arbitrary beam structures with arbitrary boundary conditions, *Journal of Sound and Vibration* (2006).
[19] S.M. Wiedemann, Dynamics and Control of Flexible Articulated Space Manipulators with Large Payloads, PhD Thesis, Cranfield University, UK, 2001.
[20] S.M. Wiedemann, C.L. Kirk, Dynamic analysis of flexible space shuttle remote manipulator system with large payloads, *Proceedings of the Fifth International Conference on Dynamics and Control of Structures and Systems in Space*, Cambridge University, 2002.